Article

Discovery Medicine 2026; 38(207): 1260–1273
https://doi.org/10.24976/Discov.Med.202638207.100

Impaired Viability Improvement and Suppression of Ferroptosis and Mitochondria Dysfunction in DHEA-Treated Ovarian Granulosa Cells in Polycystic Ovary Syndrome by HMGB1 Deficiency via Nrf2 Activation

Yuhong Yang[1], Lin Ma[1,*], Jian Huang[1], Ting Feng[1]

[1]Department of Obstetrics and Gynecology, Hangzhou Women's Hospital, 310008 Hangzhou, Zhejiang, China
*Correspondence: malin2023@hznu.edu.cn (Lin Ma)
Submitted: 7 November 2025 Revised: 3 February 2026 Accepted: 27 February 2026 Published: 20 April 2026

Background: Polycystic ovary syndrome (PCOS) is a prevalent endocrine disorder characterized by ovarian dysfunction. High mobility group box 1 (HMGB1) is elevated in PCOS and implicated in its pathogenesis, while nuclear factor E2-related factor 2 (Nrf2) is a key regulator of antioxidative defense. However, the role and mechanism of HMGB1 in PCOS, particularly its relationship with Nrf2 signaling in ovarian granulosa cell injury, remain unclear. This study aimed to investigate whether HMGB1 deficiency protects human ovarian granulosa cells from Dehydroepiandrosterone (DHEA)-induced impairments and to explore whether this protective effect is mediated through activation of the Nrf2 pathway.

Methods: In this work, a PCOS cellular model was established by treating KGN cells with 20 nM DHEA for 48 h. Then, si-HMGB1 or si-NC was transfected into KGN cells for loss-of-function experiments. To further elucidate the role of Nrf2 signaling in the HMGB1-mediated protective effect on ovarian cells, rescue experiments were performed wherein KGN cells underwent pretreatment with 10 µM Nrf2 inhibitor ML385 for 24 h before subsequent interventions.

Results: HMGB1 knockdown enhanced DHEA-treated KGN cells' impaired viability, as well as inhibited DHEA-induced ferroptosis and mitochondrial dysfunction of KGN cells ($p < 0.05$). ML385 treatment partially reversed the relieving impact of HMGB1 deficiency regarding impaired viability of ovarian granulosa cells (GCs) treated by DHEA, as well as inhibitory effects of HMGB1 deficiency on ferroptosis and mitochondrial dysfunction of ovarian GCs caused by DHEA induction ($p < 0.05$).

Conclusion: Deficiency of HMGB1 improves impaired viability of DHEA-treated GCs and suppresses ferroptosis and mitochondrial dysfunction in PCOS through Nrf2 activation.

Keywords: ovarian granulosa cells; HMGB1; Nrf2; DHEA; polycystic ovary syndrome

Introduction

Polycystic ovary syndrome (PCOS) has been among the most prevalent endocrine-metabolic diseases in reproductive-aged females and manifests a complicated relationship of endocrine and metabolic disorders characterized by hyperandrogenism, polycystic ovaries, and ovarian dysfunction [1,2]. A large number of studies have indicated abnormal earlier follicle growth and impaired follicle development as major parameters of PCOS' ovulation dysfunctions [3,4]. Ovarian Granulosa Cells (GCs), the vital somatic ovarian part, contribute to forming follicle microenvironments and have crucial functions in transiting from primordial to mature follicles [5,6]. Hence, a thorough grasp of GC dysfunction in PCOS pathogenesis is of high urgency.

HMGB1 (high mobility group box 1) has wider expression as a member of the HMG family. It is a non-histone DNA-binding protein possessing multiple biological functions. It interacts with chemokines, cytokines, and molecular patterns associated with pathogens [7,8]. A series of researches have reported a high level of HMGB1 in serum and ovaries of PCOS carrying women [9,10]. Importantly, HMGB1's positive expression levels have been found to contribute to PCOS [11–13]. Cryptotanshinone can alleviate rats' PCOS via the inhibition of HMGB1/TLR4/NF-κB molecular pathway [11]. lncRNA ZFAS1 down-regulation can show binding towards microRNA-129 for suppressing the expression of HMGB1, which in turn inhibits GCs apoptosis in PCOS, promotes proliferation, and suppresses endocrine disturbances [12]. Emodin can improve ovarian functions and glucose metabolic patterns in mice having PCOS by inactivating the HMGB1/TLR4/NF-κB signaling pathway [13].

Nrf2 (nuclear factor E2-related factor 2), being a key transcriptional parameter, is the reason for antioxidant de-

fense and cellular redox balance [14]. Abundant studies have revealed that the Nrf2 pathway has a protective role in diverse diseases, including PCOS [15–18]. Carnosol can inhibit ovarian GCs apoptosis and oxidative stress, and attenuate PCOS phenotype in mice by activating the Nrf2/HO-1 pathway mediated by Keap1 [15]. Inhibition of NOX4 can mitigate oxidative stress and apoptosis of ovarian GCs in PCOS rats through activation of the Nrf2/HO-1 pathway [16]. Salidroside can alleviate apoptosis and oxidative stress in dihydrotestosterone-treated ovarian GCs via activating AMPK/Nrf2 pathway [17]. Sulforaphane can protect ovarian GCs from oxidative stress and apoptosis in PCOS patients via the AMPK/AKT/Nrf2 pathway activation [18].

In current research, KGN cells treated by DHEA have been developed as the PCOS cellular model, and the protective effects of HMGB1 deficiency in PCOS were explored regarding three parameters: ovarian GCs' viability, ferroptosis, and mitochondrial dysfunction. Moreover, whether the Nrf2 signaling pathway could participate in HMGB1 deficiency-mediated protective effects against PCOS was thoroughly elucidated.

Materials and Methods

Cells Culture

The human ovarian granulosa cell line KGN was obtained from the Cell Bank of the Chinese Academy of Sciences (SCSP-5495, Shanghai, China). Cells were cultured in Dulbecco's Modified Eagle Medium (DMEM; Gibco, Cat. No. 11995065) supplemented with 10% Fetal Bovine Serum (FBS; Gibco, Cat. No. 10099141) and 1% penicillin-streptomycin solution (Beyotime, Cat. No. C0222). Cells were maintained in a humidified incubator at 37 °C with 5% CO_2. For routine passaging and experiments, cells were seeded in appropriate culture vessels (e.g., 6-well plates, 25 cm^2 flasks) and grown to 70–80% confluence before subsequent treatments or transfection. The cell line was authenticated by short tandem repeat (STR) profiling and confirmed to be free of mycoplasma contamination. All experiments were performed with mycoplasma-free cells within 10 passages after resuscitation.

Cells Treatment

KGN cells were seeded in 6-well plates (Corning, Cat. No. 3516) at a density of 2×10^5 cells per well and allowed to adhere overnight. The following day, cells were treated with various concentrations of DHEA (MedChemExpress, Cat. No. HY-14650; dissolved in Dimethyl Sulfoxide [DMSO, Sigma, Cat. No. D2650]) at 0, 2.5, 5, 10, 20, and 40 nM. The final concentration of DMSO in the culture medium was maintained below 0.1% (v/v) in all groups, including the vehicle control. Cells were incubated with DHEA in a humidified incubator at 37 °C with 5% CO_2 for 48 hours. After the treatment period, cells or culture supernatants were harvested for subsequent analyses as described in the respective experimental sections. The negative control siRNA (si-NC) and two distinct siRNA plasmids targeting human HMGB1 (si-HMGB1#1, si-HMGB1#2) were designed and synthesized by GenePharma (Shanghai, China). For the Nrf2 inhibition experiments, KGN cells were pretreated with 10 μM of the specific Nrf2 inhibitor ML385 (MedChemExpress, Cat. No. HY-100523) or an equal volume of vehicle (DMSO) for 24 hours prior to subsequent DHEA exposure and/or transfection procedures.

Cells Transfection

KGN cells were seeded in 6-well plates (Corning, Cat. No. 3516) at a density of 1.5×10^5 cells per well and cultured for approximately 24 hours until they reached 60–70% confluence. Transfection was then performed using Lipofectamine® 2000 reagent (Invitrogen, Cat. No. 11668019) according to the manufacturer's instructions. Briefly, for each well, 100 pmol of siRNA was diluted in 250 μL of Opti-MEM® I Reduced Serum Medium (Gibco, Cat. No. 31985070). In a separate tube, 5 μL of Lipofectamine® 2000 was mixed with 250 μL of Opti-MEM® and incubated for 5 minutes. The two solutions were then combined, gently mixed, and incubated for an additional 20 minutes to allow for complex formation. The resulting siRNA-lipid complexes (500 μL total volume) were added dropwise to each well containing cells and 1.5 mL of fresh, antibiotic-free culture medium. The cells were incubated with the transfection complexes for 6 hours at 37 °C, after which the medium was replaced with fresh complete growth medium. Cells were harvested for subsequent experiments 48 hours post-transfection to assess knockdown efficiency or for further treatments. The siRNA sequences were as follows: si-HMGB1#1: sense 5′-GCUGAAGAAGAAGAACUUUTT-3′, antisense 5′-AAAGUUCUUCUUCUUCAGCTT-3′; si-HMGB1#2: sense 5′-GGAUCUGAAGAAGCUCUAATT-3′, antisense 5′-UUAGAGCUUCUUCAGAUCCTT-3′; si-NC: sense 5′-UUCUCCGAACGUGUCACGUTT-3′, antisense 5′-ACGUGACACGUUCGGAGAATT-3′.

RT-qPCR

Total RNA was extracted from KGN cells using TRIzol Reagent. cDNA was synthesized from the RNA using PrimeScript™ RT Kit (RR047A, Takara, Tokyo, Japan). Quantitative PCR was performed on an Applied Biosystems 7300 (ABI, MA, USA) using TB Green® Premix Ex Taq™ II, with GAPDH serving as the internal control. The 20 μL PCR reaction system consisted of 10 μL TB Green Premix Ex Taq II (2X, RR820A, TB Green® Premix, Takara, Tokyo, Japan), 0.8 μL each of forward and reverse primers (10 μM), 2 μL cDNA template, and 6.4 μL RNase-free water. The thermal cycling parameters were as follows: initial denaturation at 95 °C for 30 seconds, followed by 40 cy-

cles of 95 °C for 5 seconds and 60 °C for 30 seconds. Relative *HMGB1* gene expressions underwent normalization to *GAPDH* and calculations were made via $2^{-\Delta\Delta Ct}$ methodology. Forward (F) and reverse (R) primers are shown below. *HMGB1*-F 5′-AGATATGGCAAAAGCGGACA-3′ and *HMGB1*-R 5′-GGGCGATACTCAGAGCAGAAG-3′, *GAPDH*-F: 5′-GTCTCCTCTGACTTCAACAGCG-3′, *GAPDH*-R: 5′-ACCACCCTGTTGCTGTAGCCAA-3′.

Western Blotting

Total protein concentrations extracted from KGN cells using RIPA buffer were determined via BCA assay. Proteins (30 µg/lane) were fractionated by SDS-PAGE and transferred onto PVDF membranes. Non-specific binding sites were blocked with 5% BSA. Primary antibodies against HMGB1 (Cusabio, China, CSB-RA439052A0HU, 1:1000), Acyl-CoA Synthetase Long Chain Family Member 4 (ACSL4, Beyotime, China, AG1908, 1:1000), Glutathione Peroxidase 4 (GPX4) (Fusheng, China, AK19118, 1:1000), Ferritin Heavy Chain 1 (FTH1, Cell Signaling Technology, USA, 4393, 1:1000), SLC7A11 (Selleck, China, F0517, 1:1000), Nuclear Nrf2 (Cell Signaling Technology, China, #12721, 1:1000), Nrf2 (#12721, 1:1000), Histone H3 (Fusheng, China, AK1138, 1:1000) and GAPDH (Leading Biology, China, AMM22088N, 1:500) underwent incubation overnight at 4 °C with PVDF membranes. After washing, the membranes were incubated with horseradish peroxidase (HRP)–conjugated goat anti-rabbit secondary antibody (Beyotime, China, Cat. No. A0208, 1:2000) or HRP-conjugated goat anti-mouse secondary antibody (Beyotime, China, Cat. No. A0216, 1:2000) for 1 hour at room temperature. Loading controls had been GAPDH and Histone H3. The ECL kit was employed to develop protein signals, and the protein bands were quantified using Image J 5.0 (National Institutes of Health, USA).

CCK-8 Assays

The 96-well plates were employed to culture 5×10^3 KGN cells per well in standardized conditions, followed by incubation for 4 h with CCK-8 solution (10 µL, Beyotime, Shanghai). The absorbance of each well was measured using a microplate reader (Bio-Rad, CA, USA) at 450 nm.

Measurement of Total Iron

Total iron levels in KGN cells were measured using an Iron Assay Kit (Jiancheng Bioengineering Institute, Nanjing, China, Cat. No. A039-2-1) according to the manufacturer's instructions. Briefly, KGN cells were seeded in 6-well plates at a density of 2×10^5 cells per well and subjected to the respective treatments. After treatment, cells were collected, thoroughly homogenized, and centrifuged at 1000 ×g at 4 °C for 10 minutes to obtain the supernatant. The supernatant was then mixed with the kit reagents and incubated at 37 °C for 10 minutes. The absorbance was measured at a wavelength of 520 nm using a microplate reader (Bio-Rad, Model 680). The total iron concentration in the samples was calculated based on a standard curve generated from iron standards provided in the kit. The results were normalized to the total protein concentration of the corresponding sample, which was determined by a BCA protein assay kit, and expressed as nmol per mg of protein.

4-Hydroxynonenal (HNE) and MDA Measurements

The levels of lipid peroxidation products, Malondialdehyde (MDA) and 4-Hydroxynonenal (4-HNE), in KGN cells were quantified using a commercial Lipid Peroxidation (MDA) Assay Kit (Jiancheng Bioengineering Institute, Nanjing, China, Cat. No. A003-1-2) and a 4-HNE ELISA Kit (Jiancheng Bioengineering Institute, Cat. No. H268-1-2), respectively, following the manufacturers' protocols.

ROS Measurements

Intracellular ROS levels were detected using the fluorescent probe 2′,7′-Dichlorofluorescin-diacetate (DCFH-DA; Beyotime, Shanghai, China, Cat. No. S0033S). KGN cells were seeded in 24-well plates (Corning, Cat. No. 3524) at a density of 5×10^4 cells per well. After treatments, cells were washed twice with phosphate-buffered saline (PBS) and then incubated with 10 µM DCFH-DA (diluted in serum-free DMEM) in the dark at 37 °C for 30 minutes, followed by imaging of stained cells under a fluorescent microscope (Leica, Wetzlar, Germany). Image J was employed to calculate fluorescent intensities.

Lipid ROS Measurements

Intracellular lipid ROS generation was assessed using the fluorescent probe BODIPY™ 581/591 C11 (Thermo Fisher Scientific, USA, Cat. No. D3861). KGN cells were seeded in 24-well plates at a density of 5×10^4 cells per well. Intracellular lipids ROS generation was detected via BODIPY 581/591 C11 probe by incubating KGN cells in the dark for 30 min at 37 ℃. Cells after staining had been imaged using fluorescent microscopy. The fluorescence intensity of the oxidized (green) and non-oxidized (red) forms was measured from at least five random fields per well using ImageJ software (National Institutes of Health, USA), and the degree of lipid peroxidation was quantified and expressed as the ratio of green to red fluorescence intensity.

Staining by JC-1

JC-1 staining kit (Beyotime, Shanghai, China, Cat. No. C2006) was employed to detect mitochondrial membrane potential (MMP). KGN cells were seeded in 24-well plates at 5×10^4 cells per well. KGN cells underwent incubation with the JC-1 reagent at 37 °C for 20 min in the dark, followed by washing twice with JC-1 staining buffer. Stained cells were imaged under fluorescent microscopy.

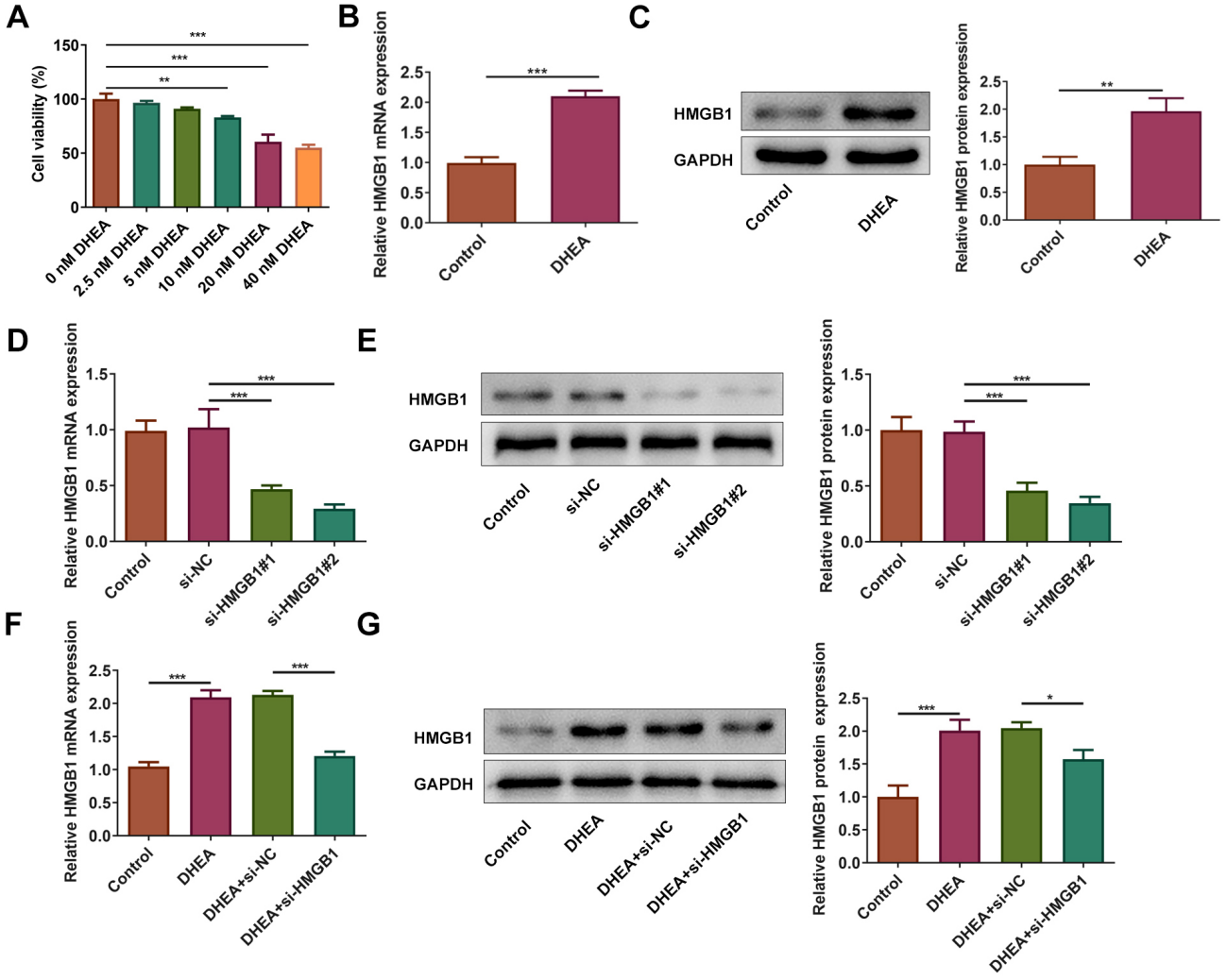

Fig. 1. Higher expression of HMGB1 in ovarian GCs treated by DHEA. (A) Various DHEA concentrations (0, 2.5, 5, 10, 20, 40 nM) were utilized to treat KGN cells for 48 h. The CCK-8 assay was employed to detect KGN cells' viability. (B,C) 20 nM DHEA used to treat KGN cells. Western blotting and RT-qPCR were employed to detect HMGB1 protein and mRNA expression levels. (D,E) si-HMGB1#1, si-HMGB1#2 or si-N were utilized to transfect KGN cells. Western blotting and RT-qPCR were applied to detect HMGB1 mRNA expression for testing transfection efficiencies. (F,G) si-NC or si-HMGB1 were used to transfect KGN cells treated by DHEA. Western blotting and RT-qPCR were utilized to detect HMGB1 mRNA expression. Each experiment was repeated for three times. * $p < 0.05$, ** $p < 0.01$, *** $p < 0.001$. HMGB1, High Mobility Group Box 1; GCs, Granulosa Cells; DHEA, Dehydroepiandrosterone; CCK-8, cell counting kit-8; si-NC, negative control siRNA.

Measurements of Mitochondrial ROS

KGN cells were seeded in 24-well plates at 5×10^4 cells per well. MitoSOX™ Red mitochondrial superoxide indicator (Yeasen, Shanghai, China, Cat. No. 40778ES50) was applied to detect mitochondria ROS. Hank's balanced salt solution (HBSS) was utilized to wash KGN cells, followed by incubation with MitoSOX Red (5 µM) in the dark at 37 °C for 15 min. The stained cells were imaged under fluorescent microscopy.

Measurement of Mitochondrial Permeability Transition Pore (mPTP)

The opening of the mitochondrial permeability transition pore (mPTP) was assessed using the calcein-AM/cobalt chloride ($CoCl_2$) quenching method. KGN cells were seeded in 24-well plates (Corning, Cat. No. 3524) at a density of 5×10^4 cells per well. After the respective treatments, cells were washed twice with PBS. Cells were then loaded with 1 µM calcein-AM (MedChemExpress, Cat. No. HY-D0041) and 1 mM $CoCl_2$ (Sigma, Cat. No. 60818) simultaneously, and incubated in the dark at 37 °C for 20 minutes. This procedure was followed by an additional 30-minute incubation with 1 mM $CoCl_2$ alone to thoroughly

quench the cytosolic and nuclear calcein fluorescence. After incubation, cells were washed three times with PBS to remove excess probes. Stained cells were pictured by fluorescence microscopy.

Oxygen Consumption Rate (OCR) Detection

Cellular oxygen consumption rate (OCR) was measured using the Seahorse XF Cell Mito Stress Test Kit (Agilent, USA, Cat. No. 103015-100). KGN cells were seeded in XF96 cell culture microplates (Agilent, Cat. No. 101085-004) at a density of 1.5×10^4 cells per well and cultured for 24 hours to allow for adherence. One hour prior to the assay, the culture medium was replaced with pre-warmed, pH-adjusted XF Base Medium (Agilent, Cat. No. 103334-100) supplemented with 1 mM pyruvate, 2 mM glutamine, and 10 mM glucose, and the cells were incubated in a non-CO_2 incubator at 37 °C. During the assay, the following mitochondrial inhibitors from the kit were sequentially injected into each well to achieve the final concentrations indicated: oligomycin (1.5 µM), FCCP (1.0 µM), and a mixture of rotenone (0.5 µM) and antimycin A (0.5 µM). The OCR was measured in real-time using a Seahorse XF96 Extracellular Flux Analyzer (Agilent). Key parameters of mitochondrial function, including basal respiration, Adenosine Triphosphate (ATP)-linked respiration, maximal respiration, and spare respiratory capacity, were calculated from the OCR profile according to the manufacturer's instructions. The results from each well were normalized to the total protein content determined by a BCA assay post-measurement.

Statistical Analyses

Statistical analyses were performed using GraphPad Prism software (version 8.0; GraphPad Software, San Diego, CA, USA). Data from three independent experiments are presented as mean ± standard deviation (SD). Statistical comparisons between multiple groups were performed using one-way analysis of variance (ANOVA) followed by Tukey's post-hoc test, unless otherwise specified. For the oxygen consumption rate (OCR) measurements, data were analyzed using repeated-measures ANOVA followed by Bonferroni's post-hoc test. Comparisons between two groups were conducted using an unpaired Student's *t*-test. A *p*-value of less than 0.05 was considered statistically significant.

Results

Higher Expression of HMGB1 in Ovarian GCs Treated by DHEA

Various DHEA concentrations (0, 2.5, 5, 10, 20, 40 nM) were utilized to treat KGN cells for 48 h. DHEA treatment based on the dosage decreased KGN cells' viability, and a PCOS cellular model was established by choosing 20 nM DHEA as the feasible dosage (Fig. 1A, $p < 0.01$). The selection of 20 nM DHEA, rather than 10 nM, was a deliberate choice to establish a robust and consistent cellular model of PCOS. Besides, a PCOS cellular model induced by DHEA had high expression of HMGB1 (Fig. 1B,C, $p < 0.01$). Afterwards, si-HMGB1#2, si-HMGB1#1, or si-NC were transfected into KGN cells to perform loss-of-function experiments targeting HMGB1. Follow-up experiments were conducted using si-HMGB1#2, which exhibited optimum transfection potential (Fig. 1D,E, $p < 0.001$). It was observed that knockdown of HMGB1 reversed the enhanced HMGB1 expression in ovarian KGN cells treated by DHEA (Fig. 1F,G, $p < 0.05$).

Improvement in Impaired Viability of Ovarian GCs Treated by DHEA via HMGB1 Deficiency

KGN cells' viability was impaired by the treatment of DHEA, whereas HMGB1 knockdown restored cell viability in DHEA-treated KGN cells (Fig. 2, $p < 0.05$).

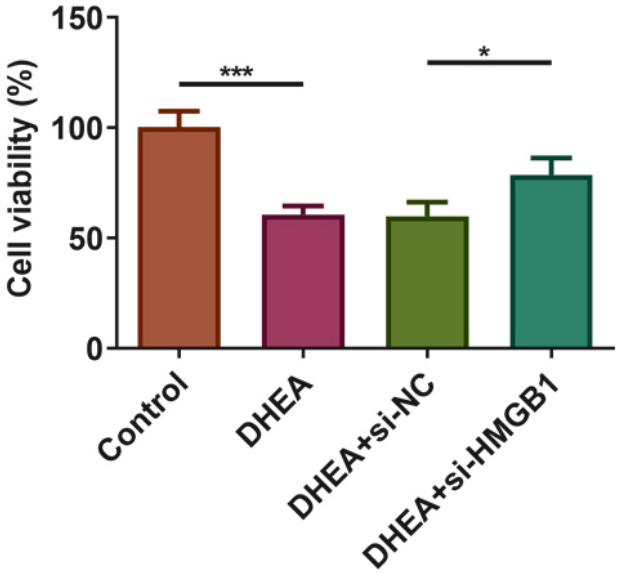

Fig. 2. HMGB1 deficiency improves the impaired viability of ovarian GCs treated by DHEA. KGN cells treated by DHEA were transfected with si-NC or si-HMGB1. The CCK-8 assay was utilized to detect KGN cells' viability. Each experiment was repeated for three times. * $p < 0.05$, *** $p < 0.001$.

HMGB1 Deficiency Inhibits DHEA-Induced Ferroptosis of Ovarian GCs

To determine whether HMGB1 participates in DHEA-induced ferroptotic injury in ovarian granulosa cells, multiple biochemical and molecular markers of ferroptosis were systematically evaluated. As shown in Fig. 3A, DHEA treatment markedly increased intracellular total iron accumulation in KGN cells, whereas HMGB1 knockdown significantly reduced iron levels compared with the DHEA + si-NC group, indicating attenuation of iron overload. Lipid

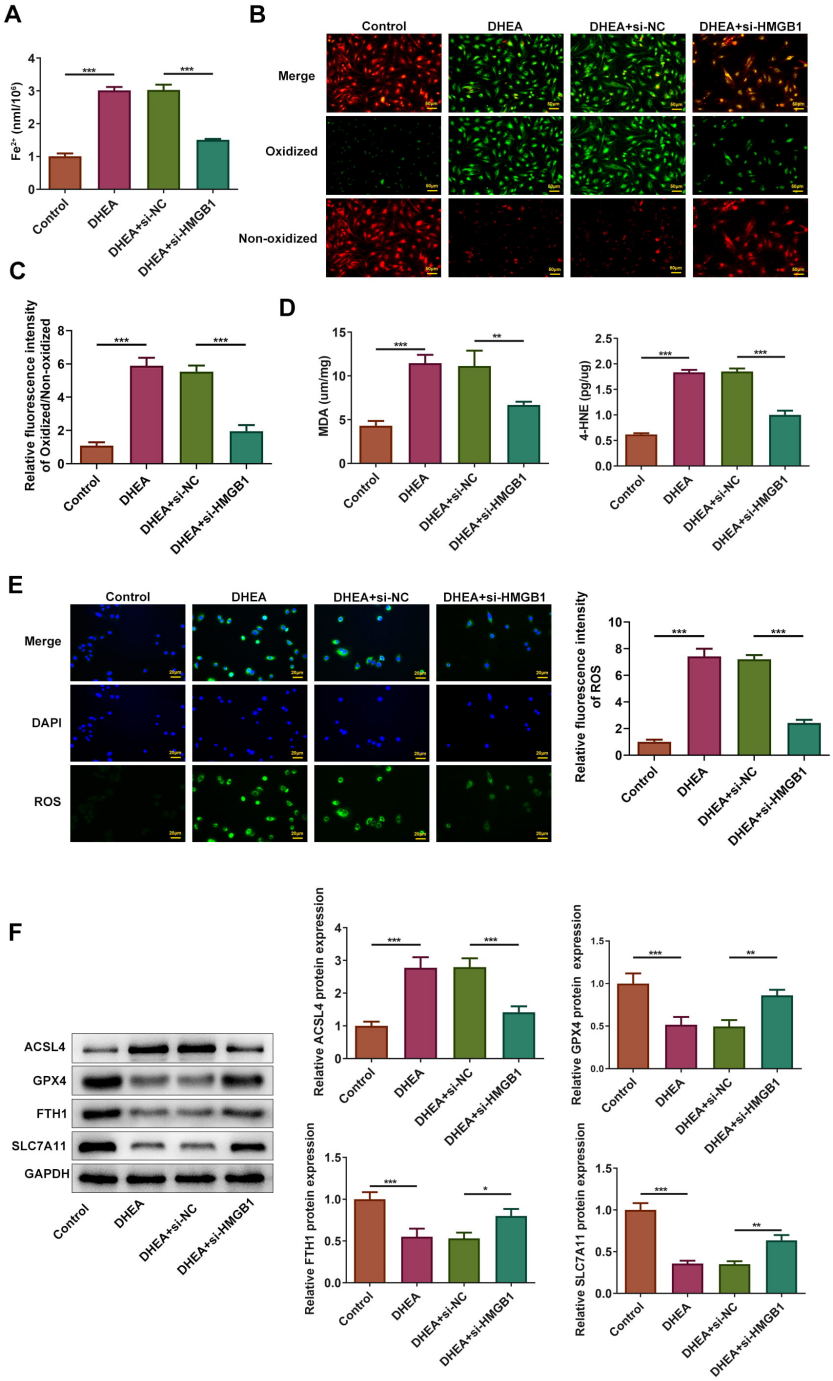

Fig. 3. HMGB1 deficiency inhibits ovarian GCs' ferroptosis induced by DHEA. si-NC or si-HMGB1 were employed to transfect KGN cells treated by DHEA. (A) Intracellular total iron levels were measured using a colorimetric iron assay kit. (B) Lipid peroxidation was assessed using the BODIPY 581/591 C11 probe; representative images of merged signals, oxidized (green), and non-oxidized (red) fluorescence are shown (scale bar = 50 μm). (C) Quantification of lipid ROS levels expressed as the ratio of oxidized to non-oxidized fluorescence intensity. (D) Levels of lipid peroxidation products Malondialdehyde (MDA) and 4-Hydroxynonenal (4-HNE) were determined using commercial assay kits. (E) Intracellular reactive oxygen species (ROS) generation was detected by DCFH-DA staining; representative fluorescence images and quantitative analysis are shown (scale bar = 20 μm). (F) Protein expression levels of ferroptosis-related markers ACSL4, GPX4, FTH1, and SLC7A11 were analyzed by western blotting, with GAPDH as the loading control, followed by densitometric quantification. Data are presented as mean ± SD from three independent experiments. $*p < 0.05$, $**p < 0.01$, $***p < 0.001$. ROS, Reactive Oxygen Species; DCFH-DA, 2′,7′-Dichlorofluorescin-diacetate; ACSL4, Acyl-CoA Synthetase Long Chain Family Member 4; GPX4, Glutathione Peroxidase 4; FTH1, Ferritin Heavy Chain 1; SLC7A11, Solute Carrier Family 7 Member 11; GAPDH, glyceraldehyde-3-phosphate dehydrogenase.

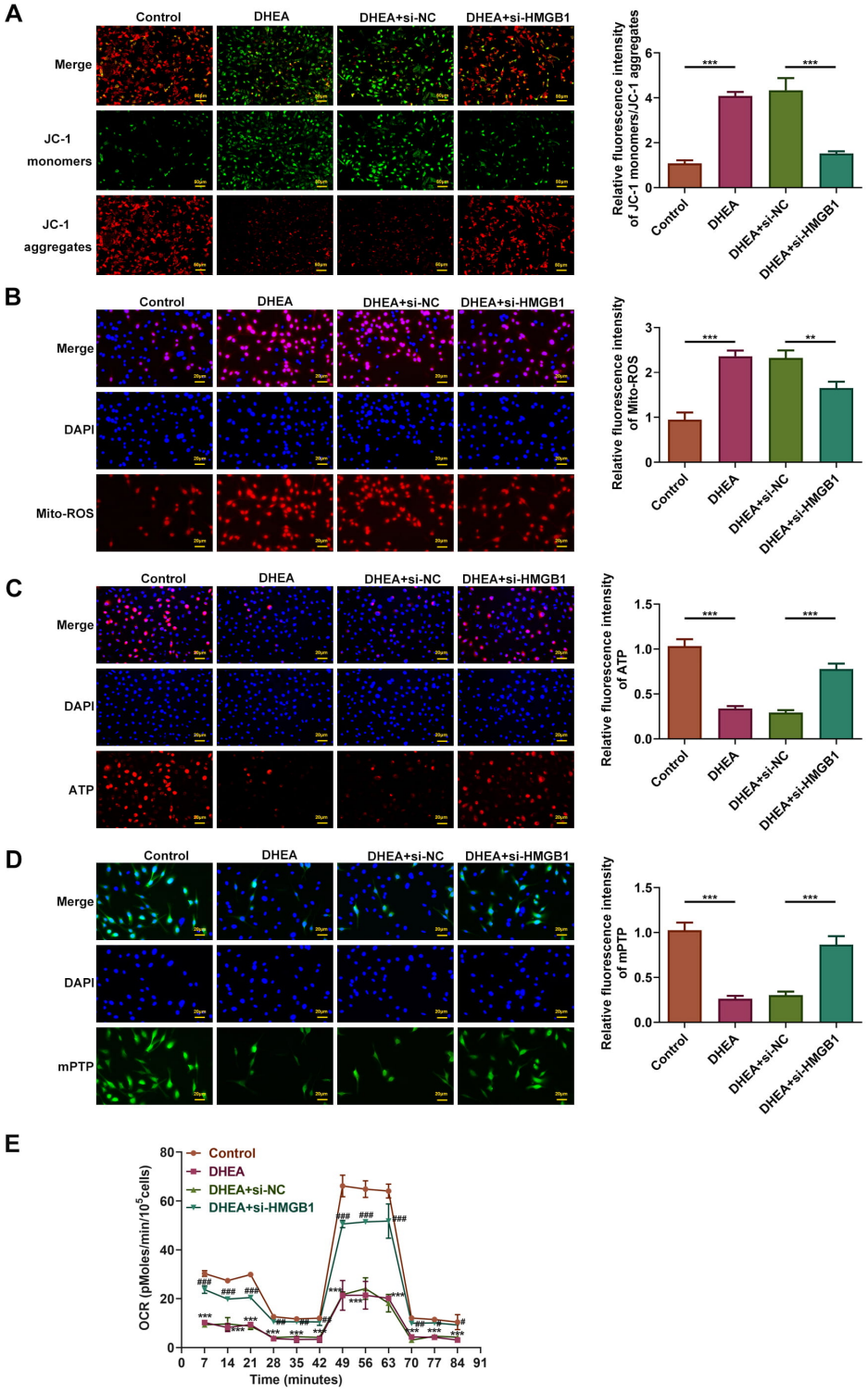

Fig. 4. Deficiency of HMGB1 causes suppression of ovarian GCs mitochondrial dysfunction induced by DHEA. si-NC or si-HMGB1 were utilized to transfect KGN cells treated by DHEA. (A) JC-1 was applied to detect MMP. (B) Mitochondrial ROS generation was detected by MitoSOX Red probes. (C) ATP assay kit was applied to detect ATP content. (D) mPTP was detected by calcein-AM fluorescence probe. (E) The cellular OCR was determined using Cell Mito Stress Test Kit. Data were analyzed by repeated-measures ANOVA (n = 3 independent experiments). ** $p < 0.01$, *** $p < 0.001$ vs Control, $^{\#}p < 0.05$, $^{\#\#}p < 0.01$, $^{\#\#\#}p < 0.001$ vs DHEA+si-NC group. JC-1, 5,5',6,6'-Tetrachloro-1,1',3,3'-tetraethylbenzimidazolocarbocyanine iodide; MMP, mitochondrial membrane potential; ATP, Adenosine Triphosphate; mPTP, Mitochondrial Permeability Transition Pore; OCR, Oxygen Consumption Rate; ANOVA, Analysis of Variance.

peroxidation, a hallmark event of ferroptosis, was further assessed using the BODIPY 581/591 C11 probe. DHEA exposure caused a pronounced shift from red (non-oxidized) to green (oxidized) fluorescence, reflecting excessive lipid ROS generation (Fig. 3B). Quantitative analysis confirmed a significant elevation in the oxidized/non-oxidized fluorescence ratio following DHEA treatment, which was markedly suppressed upon HMGB1 silencing (Fig. 3C, $p < 0.001$). Consistently, DHEA significantly increased the levels of lipid peroxidation end products MDA and 4-HNE, while HMGB1 deficiency substantially reduced their accumulation (Fig. 3D, $p < 0.01$). Moreover, DCFH-DA staining revealed that intracellular ROS production was strongly enhanced by DHEA, an effect that was effectively mitigated by HMGB1 knockdown (Fig. 3E, $p < 0.001$). At the molecular level, western blot analysis demonstrated that DHEA treatment upregulated the pro-ferroptotic protein ACSL4 while downregulating key anti-ferroptotic regulators GPX4, FTH1, and SLC7A11 (Fig. 3F, $p < 0.05$). Importantly, HMGB1 deficiency reversed these alterations, characterized by reduced ACSL4 expression and restored GPX4, FTH1, and SLC7A11 levels. Collectively, these findings indicate that HMGB1 plays a critical role in mediating DHEA-induced ferroptosis in ovarian granulosa cells, and that HMGB1 deficiency effectively suppresses ferroptotic damage by limiting iron accumulation, lipid peroxidation, oxidative stress, and ferroptosis-associated protein dysregulation.

Suppression of Mitochondrial Dysfunction of Ovarian GCs Induced by DHEA via HMGB1 Deficiency

Red fluorescent aggregates were depicted by healthy mitochondria, while green fluorescent monomers were depicted by damaged mitochondria upon JC-1 staining. Increased green, fluorescent staining and weakened red fluorescent staining indicated impaired mitochondria in KGN cells treated by DHEA. HMGB1 knockdown decreased green fluorescence and increased red fluorescence in DHEA-treated KGN cells, restoring damaged mitochondria in KGN cells treated by DHEA (Fig. 4A). Meanwhile, treatment by DHEA triggered mitochondrial ROS generation, reduced ATP content, decreased the opening rate of mPTP and decreased levels of OCR, indicating that DHEA treatment caused mitochondrial dysfunction of ovarian GCs. Conversely, knockdown of HMGB1 inhibited mitochondrial ROS generation, elevated ATP content, increased the opening rate of mPTP and increased levels of OCR, also indicating that HMGB1 knockdown caused suppression in mitochondrial dysfunction induced by DHEA of ovarian GCs (Fig. 4B–E, $p < 0.05$).

Nrf2 Signaling Pathway Activation in DHEA-Treated Ovarian GCs by HMGB1 Deficiency

Vital pathway protein nuclear Nrf2 and Nrf2 were analyzed to investigate if HMGB1 deficiency might bring ovary-protecting impact through Nrf2 signaling mediation. Decreased expression of nuclear Nrf2 and Nrf2 indicated that the Nrf2 signaling pathway is inactivated in KGN cells treated by DHEA. Nevertheless, HMGB1 knockdown distinctly enhanced nuclear Nrf2 and Nrf2 expression levels in KGN cells treated by DHEA, abolishing the Nrf2 signaling pathway inactivation in DHEA-treated KGN cells. Apparently, ML385 as an Nrf2 inhibitor partly abrogated the promoting effect of HMGB1 deficiency on Nrf2 activation in ovarian GCs treated by DHEA (Fig. 5, $p < 0.01$).

HMGB1 Deficiency Improves Impaired Viability of DHEA-Treated Ovarian GCs by Activating Nrf2 Signaling Pathway

HMGB1 knockdown restored the impaired viability of KGN cells treated with DHEA. Furthermore, ML385 treatment partially reversed the protective effect of HMGB1 deficiency on impaired viability of ovarian GCs treated by DHEA (Fig. 6, $p < 0.05$).

HMGB1 Deficiency Inhibits Ovarian GCs DHEA-Induced Ferroptosis by the Nrf2 Pathway Activation

To further clarify whether Nrf2 signaling mediates the suppressive effect of HMGB1 deficiency on ferroptosis, KGN cells were treated with the specific Nrf2 inhibitor ML385 following HMGB1 knockdown. As shown in Fig. 7A, HMGB1 deficiency significantly reduced intracellular iron accumulation induced by DHEA, whereas ML385 treatment partially restored iron levels, indicating reactivation of iron overload upon Nrf2 inhibition. Consistently, BODIPY 581/591 C11 staining revealed that inhibition of Nrf2 markedly increased lipid ROS generation in HMGB1-deficient cells, as evidenced by enhanced green fluorescence and a higher oxidized/non-oxidized fluorescence ratio compared with the DHEA + si-HMGB1 group (Fig. 7B,C, $p < 0.001$). These findings suggest that Nrf2 activity is required for HMGB1 deficiency–mediated suppression of lipid peroxidation. In line with these observations, ML385 treatment significantly elevated the levels of lipid peroxidation end products MDA and 4-HNE, partially reversing their reduction caused by HMGB1 knockdown in DHEA-treated cells (Fig. 7D, $p < 0.05$). Moreover, intracellular ROS levels, which were markedly decreased by HMGB1 deficiency, were substantially restored upon Nrf2 inhibition, as demonstrated by DCFH-DA staining and quantitative fluorescence analysis (Fig. 7E, $p < 0.001$). At the molecular level, western blot analysis showed that ML385 treatment partially abrogated the HMGB1 deficiency–induced downregulation of the pro-ferroptotic protein ACSL4, while simultaneously reducing

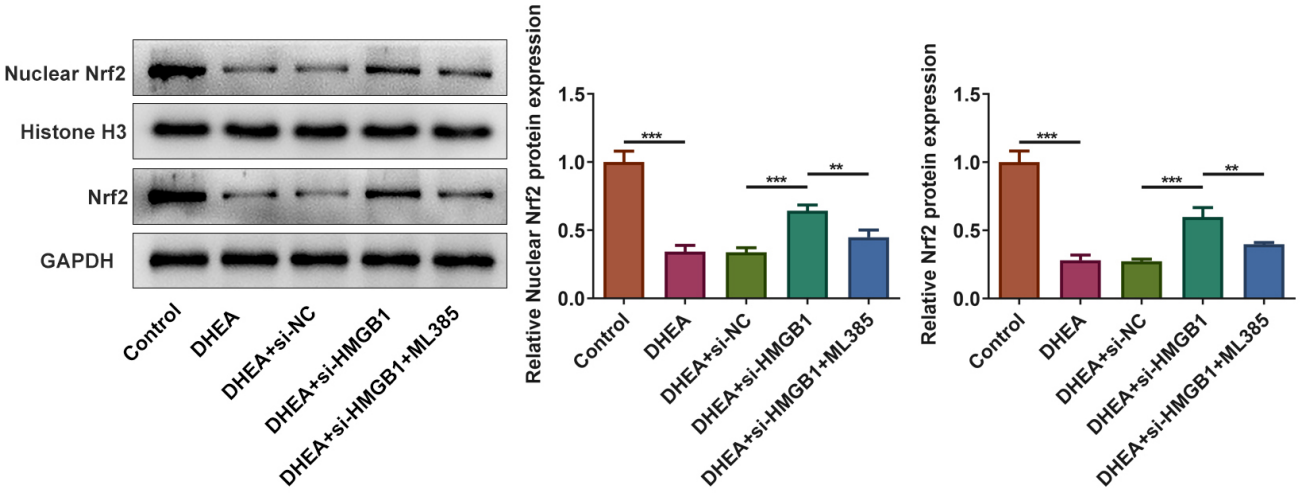

Fig. 5. HMGB1 deficiency activates Nrf2 signaling pathway in ovarian GCs treated by DHEA. si-NC or si-HMGB1 were utilized to transfect KGN cells treated by DHEA. Western blotting was employed to detect expression levels of nuclear Nrf2 and Nrf2. ** $p <$ 0.01, *** $p < 0.001$. Nrf2, Nuclear Factor Erythroid 2-Related Factor 2.

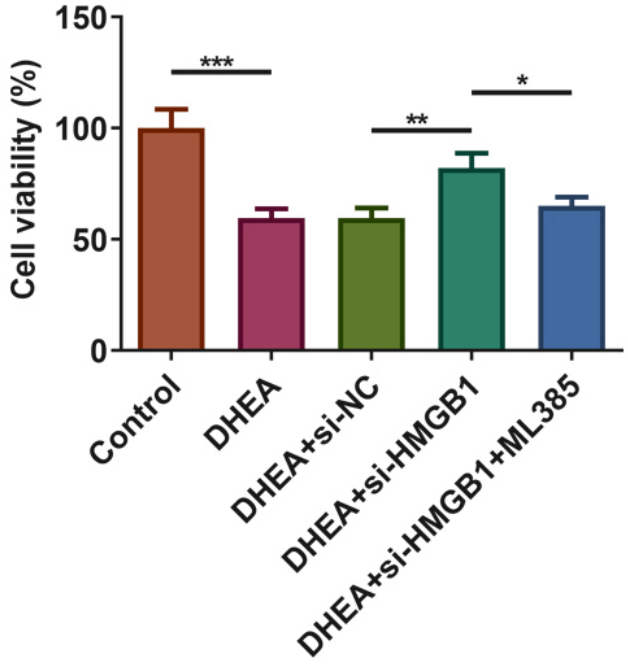

Fig. 6. Deficiency of HMGB1 enhances impaired viability of DHEA-treated ovarian GCs by activating the Nrf2 signaling pathway. si-NC or si-HMGB1 were utilized to transfect KGN cells treated by DHEA. ML385, as an Nrf2 inhibitor, was used to pretreat KGN cells for 24 h. The CCK-8 assay was applied to detect KGN cells' viability. Each experiment was repeated for three times. * $p < 0.05$, ** $p < 0.01$, *** $p < 0.001$.

the expression of anti-ferroptotic proteins GPX4, FTH1, and SLC7A11 (Fig. 7F, $p < 0.05$). These results indicate that activation of Nrf2 is essential for maintaining the ferroptosis-resistant phenotype conferred by HMGB1 deficiency. To sum up, the Nrf2 signaling pathway might partially abrogate the inhibitory impact of HMGB1 deficiency on ovarian GCs' ferroptosis induced by DHEA.

HMGB1 Deficiency Suppresses DHEA-Induced Mitochondrial Dysfunction of Ovarian GCs by Activating the Nrf2 Signaling Pathway

ML385 treatment enhanced green fluorescence staining and weakened red fluorescence staining, partly reversing the suppressive effects of HMGB1 deficiency on mitochondrial dysfunction KGN cells treated by DHEA (Fig. 8A, $p < 0.01$). Moreover, treatments by ML385 enhanced mitochondrial ROS generation, reduced ATP content, decreased the opening rate of mPTP and decreased levels of OCR, also reflecting that treatment by ML385 partly reversed the suppressive effects of HMGB1 deficiency on mitochondrial dysfunction of ovarian GCs caused by DHEA induction (Fig. 8B–E, $p < 0.05$). To sum up, the Nrf2 signaling pathway might partially abrogate the suppressive impact of HMGB1 deficiency on DHEA-induced mitochondrial dysfunction of ovarian GCs.

Discussion

PCOS etiological parameters remain ambiguous till now, which makes effective therapeutics and accurate diagnosis difficult for patients. The present work initially reveals the ovarian protection impact of HMGB1 deficiency in PCOS and fully elaborates the underlying mechanisms in the protective properties of HMGB1 deficiency in ovarian GCs for DHEA injury. The concentration range was chosen to establish a dose-response relationship and to identify a submaximal effective concentration (20 nM) that robustly induces the PCOS-like phenotype for subsequent mechanistic studies, as confirmed by our initial viability assay. In our current study, HMGB1 deficiency enhanced ovarian GCs' impaired viability treated by DHEA.

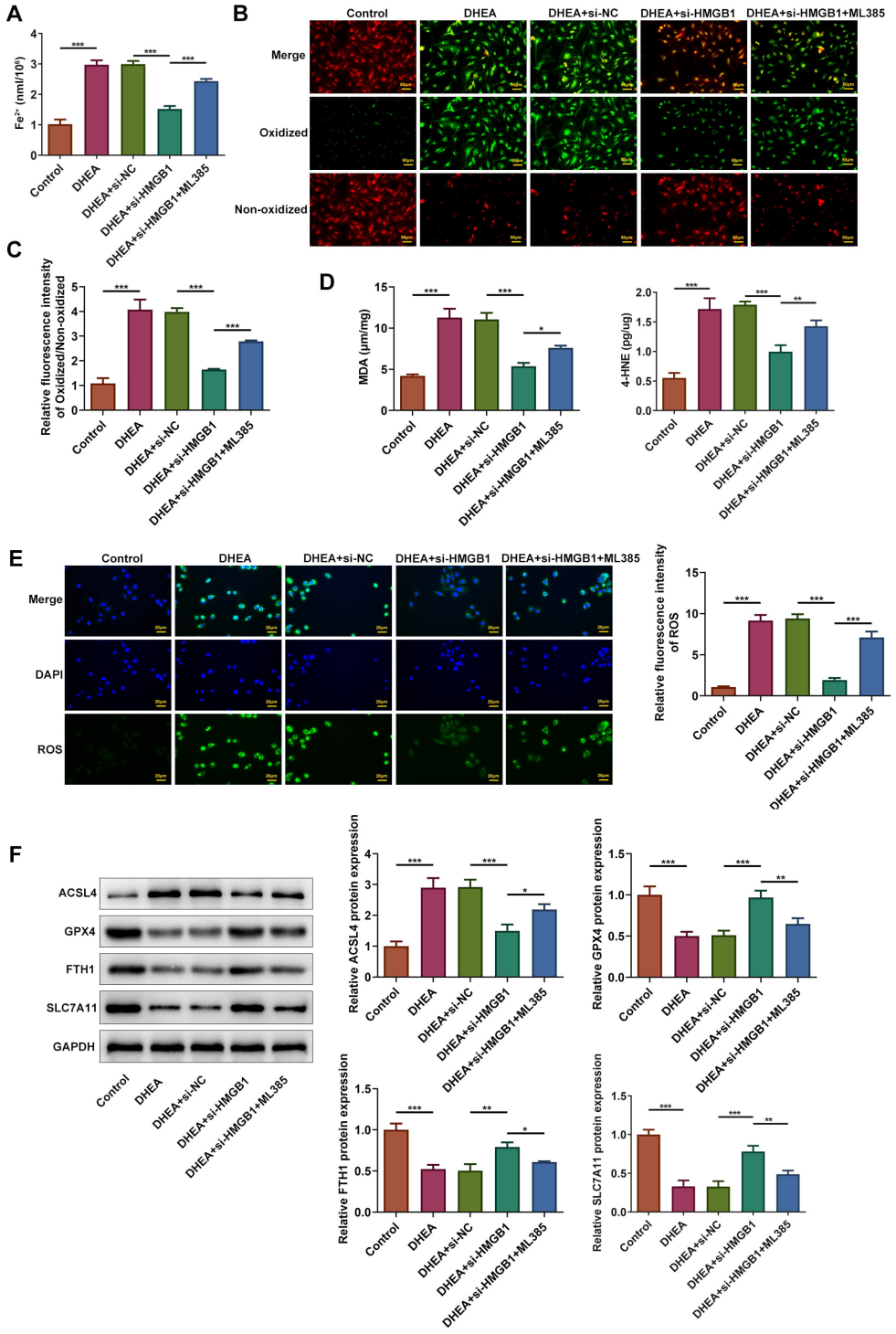

Fig. 7. HMGB1 deficiency inhibits DHEA-induced ferroptosis of ovarian GCs by activating the Nrf2 signaling pathway. si-NC or si-HMGB1 were utilized to transfect KGN cells treated by DHEA. Pretreatment of KGN cells was made for 24 h with ML385 as an Nrf2 inhibitor. (A) Intracellular total iron levels were measured using a colorimetric iron assay kit. (B) Lipid peroxidation was assessed using the BODIPY™ 581/591 C11 probe; representative images of merged signals, oxidized (green), and non-oxidized (red) fluorescence are shown (scale bar = 50 μm). (C) Quantitative analysis of lipid ROS levels expressed as the ratio of oxidized to non-oxidized fluorescence intensity. (D) Levels of Malondialdehyde (MDA) and 4-Hydroxynonenal (4-HNE) were determined as indicators of lipid peroxidation. (E) Intracellular reactive oxygen species (ROS) generation was detected by DCFH-DA staining, with representative images and fluorescence intensity quantification shown (scale bar = 20 μm). (F) Protein expression levels of ferroptosis-related markers ACSL4, GPX4, FTH1, and SLC7A11 were analyzed by western blotting, followed by densitometric quantification normalized to GAPDH. Each experiment was repeated for three times. * $p < 0.05$, ** $p < 0.01$, *** $p < 0.001$.

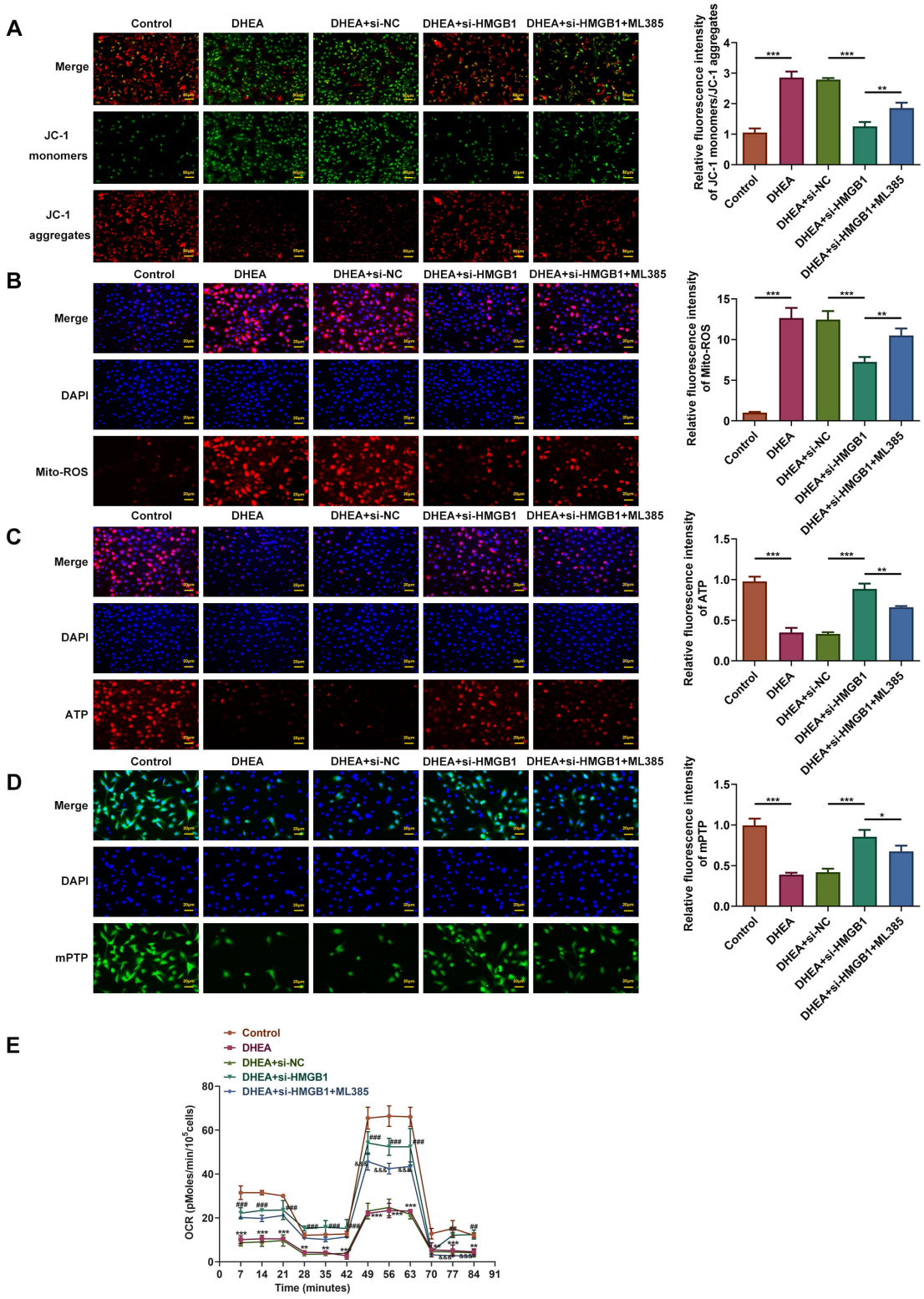

Fig. 8. Deficiency of HMGB1 causes suppression of ovarian GCs' mitochondrial dysfunction induced by DHEA via the activation of Nrf2 signaling pathway. si-NC or si-HMGB1 were employed to transfect KGN cells treated by DHEA. Pretreatment of KGN cells for 24 h with ML385 as an Nrf2 inhibitor. (A) JC-1 utilized to detect MMP. (B) MitoSOX Red probe was utilized to detect mitochondrial ROS. (C) ATP assay kit was applied to detect ATP content. (D) Calcein-AM fluorescence probe was utilized to detect mPTP. (E) The cellular OCR was detected using Cell Mito Stress Test Kit. Data were analyzed by repeated-measures ANOVA (n = 3 independent experiments). * $p < 0.05$, ** $p < 0.01$, *** $p < 0.001$ vs Control, $^{\#\#}$ $p < 0.01$, $^{\#\#\#}$ $p < 0.001$ vs DHEA+si-NC group, $^{\&\&\&}$ $p < 0.001$ vs DHEA+si-HMGB1 group.

HMGB1 participates in N-methyl-D-aspartate receptor activation-induced human umbilical vein endothelial cell ferroptosis [19]. Syringic acid can suppress skeletal muscle cells' ferroptosis for alleviating mice's ischemia/reperfusion injury of the lower limb by blocking the HMGB1 pathway [20]. HMGB1 can upregulate astrocytes' hepcidin and increase acute iron, and in turn ferroptosis in postischemic brain [21]. Overexpressed HMGB1 can promote cardiotoxicity and ferroptosis as triggered by doxorubicin in rats, though HMGB1 silencing depicted an opposite impact [22]. In this current work, HMGB1 deficiency inhibited ovarian GCs' ferroptosis induced by DHEA. Dasatinib can impair mitophagy via downregulation of keratinocytes' HMGB1 protein levels, which leads to dysfunctional mitochondrial accumulation [23]. Anti-HMGB1 rescue mitochondria dysfunctions induced by organic dust [24]. HMGB1 knockdown can suppress pancreatic cancer cells' mitochondria biogenesis induced by hypoxia [25]. HMGB1 treatment can reduce myotube mitochondria respiration and enhance ROS [26]. Propofol can protect lungs endothelial barrier functions by suppressing release of HMGB1 and HMGB1 triggered mitochondria oxidative damage [27]. In our current study, HMGB1 deficiency suppresses DHEA-induced mitochondrial dysfunction of ovarian GCs.

Spermidine can suppress ferroptosis and oxidative stress via Nrf2/HO-1/GPX4 pathway activation to alleviate ovarian damage [28]. Pterostilbene can improve ferroptosis and oxidative damage in human ovarian GCs by activating the pathway of Nrf2/HO-1 [29]. Forsythoside A mitigates Alzheimer's-linked pathologies via the inhibition of neuroinflammation mediated by ferroptosis through activation of the Nrf2/GPX4 axis [30]. Astaxanthin can activate pathway of Nrf2/HO-1 to ameliorate liver injury induced by acetaminophen, inhibit ferroptosis, and enhance autophagy [31]. Deficiency of Nrf2 can impair oxidation of mitochondria fatty acids, production of ATP, and respiration [32]. Songorine can promote cardiological mitochondria biogenesis through induction of Nrf2 in sepsis [33]. 1, 8-cineole through the Nrf2 pathway promotion can restore mitochondria functions and alleviate oxidative damage induced by OGD/R [34]. Nrf2 can maintain mitochondrial function and inhibit excessive mitochondrial division to protect against acute lung injuries induced by *S. aureus* [35]. The increase in total Nrf2 indicates its enhanced protein stability, while the concurrent rise in nuclear Nrf2 confirms its successful translocation into the nucleus. Together, these changes demonstrate a clear activation of the Nrf2 signaling pathway. Serine/threonine kinase 3 can promote mitochondrial damage and oxidative stress through induction of Nrf2 degradation in septic cardiomyopathy [36]. In our current study, it was verified that treatment by ML385 partly reversed inhibitory impact of HMGB1 deficiency on ferroptosis and mitochondrial dysfunction of ovarian GCs caused by DHEA induction. Nrf2 signaling pathway inactivation might partially abrogate inhibitory impact of HMGB1 deficiency on DHEA-induced ferroptosis and mitochondrial dysfunction of ovarian GCs.

Our study demonstrates that HMGB1 deficiency activates the Nrf2 antioxidant pathway, yet the precise upstream mechanism linking HMGB1 to Nrf2 regulation warrants further elucidation. Based on existing literature and our findings, we propose that the regulation is likely indirect, rather than involving a direct physical interaction between HMGB1 and Nrf2/Keap1. A more plausible mechanism involves HMGB1 acting as a pro-oxidant and pro-inflammatory mediator. Specifically, the release of HMGB1 can exacerbate intracellular oxidative stress and trigger inflammatory signaling pathways. This heightened oxidative stress milieu is a well-established activator of Nrf2, as reactive oxygen species can modify the cysteine residues of Keap1, leading to its dissociation from Nrf2 and subsequent Nrf2 nuclear translocation.

Limitations of this study should be noted. Firstly, our conclusions are primarily based on the KGN cell line, a human granulosa cell tumor-derived model. Although KGN cells retain many physiological characteristics and are widely used in PCOS research, their tumorigenic origin and immortalized nature may not fully recapitulate the behavior of primary ovarian granulosa cells under physiological or pathological PCOS conditions. Furthermore, a key limitation of this study is its reliance on an *in vitro* cellular model. While this approach was critical for mechanistically dissecting the HMGB1/Nrf2/ferroptosis pathway in granulosa cells, it does not recapitulate the systemic metabolic and endocrine complexities of PCOS *in vivo*. Therefore, the extrapolation of our findings to the whole organism requires caution. Future studies employing tissue-specific HMGB1 knockout mouse models, combined with hormone-induced PCOS phenotypes, will be indispensable to validate the physiological and therapeutic relevance of this pathway and to investigate its interaction with systemic metabolic disturbances.

Conclusion

To conclude, deficiency of HMGB1 enhances impaired viability of DHEA-treated GCs and suppresses ferroptosis and mitochondrial dysfunction in PCOS through the Nrf2 activation. These findings help develop reliable therapeutic clinical strategies for PCOS.

Abbreviations

4-HNE, 4-Hydroxynonenal; ACSL4, Acyl-CoA Synthetase Long Chain Family Member 4; ANOVA, Analysis of Variance; ATP, Adenosine Triphosphate; DCFH-DA, 2′,7′-Dichlorofluorescin-diacetate; DHEA, Dehydroepiandrosterone; DMEM, Dulbecco's Modified Eagle Medium; DMSO, Dimethyl Sulfoxide; FBS, Fetal Bovine Serum; FTH1, Ferritin Heavy Chain 1; GCs, Granulosa

Cells; GPX4, Glutathione Peroxidase 4; HMGB1, High Mobility Group Box 1; MDA, Malondialdehyde; mPTP, Mitochondrial Permeability Transition Pore; Nrf2, nuclear factor E2-related factor 2; OCR, oxygen consumption rate; PBS, phosphate-buffered saline; PCOS, Polycystic ovary syndrome; ROS, reactive oxygen species; SD, Standard Deviation; SLC7A11, Solute Carrier Family 7 Member 11; STR, short tandem repeat.

Availability of Data and Materials

The datasets analyzed during the current study are available from the corresponding author on reasonable request.

Author Contributions

All authors contributed to the study conception and design. Material preparation and the experiments were performed by YY. Data collection and analysis were performed by LM and JH. The first draft of the manuscript was written by TF and all authors contributed to the important editorial changes in the manuscript. All authors read and approved the final manuscript. All authors have participated sufficiently in the work to take public responsibility for appropriate portions of the content and agreed to be accountable for all aspects of the work in ensuring that questions related to its accuracy or integrity.

Ethics Approval and Consent to Participate

Not applicable.

Acknowledgment

Not applicable.

Funding

This work was supported by the Hangzhou Medical and Health Science and Technology Project (Grant No. A20251969), Mutual Fund of the Provincial Maternal and Infant Safety Research Laboratory of the Zhejiang University Women's Hospital (Grant No. ZDFY2024-MI-1) and Joint Sciencce and Technology Plan Project between the Science and Technology Department of the National Administration of Traditional Chinese Medicine and the Zhejiang Provincial Administration of Traditional Chinese Medicine (Grant No. GZY-ZJ-KJ-23089).

Conflict of Interest

The authors declare no conflict of interest.

References

[1] Azziz R. Polycystic Ovary Syndrome. Obstetrics and Gynecology. 2018; 132: 321–336. https://doi.org/10.1097/AOG.0000000000002698.

[2] Zhang W, Wu F. Linoleic acid induces human ovarian granulosa cell inflammation and apoptosis through the ER-FOXO1-ROS-NFκB pathway. Scientific Reports. 2024; 14: 6392. https://doi.org/10.1038/s41598-024-56970-x.

[3] Escobar-Morreale HF. Polycystic ovary syndrome: definition, aetiology, diagnosis and treatment. Nature Reviews. Endocrinology. 2018; 14: 270–284. https://doi.org/10.1038/nrendo.2018.24.

[4] Jarrett BY, Vanden Brink H, Oldfield AL, Lujan ME. Ultrasound Characterization of Disordered Antral Follicle Development in Women with Polycystic Ovary Syndrome. The Journal of Clinical Endocrinology and Metabolism. 2020; 105: dgaa515. https://doi.org/10.1210/clinem/dgaa515.

[5] Liu Y, Ni F, Huang J, Hu Y, Wang J, Wang X, *et al*. PPAR-α inhibits DHEA-induced ferroptosis in granulosa cells through upregulation of FADS2. Biochemical and Biophysical Research Communications. 2024; 715: 150005. https://doi.org/10.1016/j.bbrc.2024.150005.

[6] Tu J, Cheung AHH, Chan CLK, Chan WY. The Role of microRNAs in Ovarian Granulosa Cells in Health and Disease. Frontiers in Endocrinology. 2019; 10: 174. https://doi.org/10.3389/fendo.2019.00174.

[7] Chen R, Kang R, Tang D. The mechanism of HMGB1 secretion and release. Experimental & Molecular Medicine. 2022; 54: 91–102. https://doi.org/10.1038/s12276-022-00736-w.

[8] Magna M, Pisetsky DS. The role of HMGB1 in the pathogenesis of inflammatory and autoimmune diseases. Molecular Medicine (Cambridge, Mass.). 2014; 20: 138–146. https://doi.org/10.2119/molmed.2013.00164.

[9] Cirillo F, Catellani C, Sartori C, Lazzeroni P, Morini D, Nicoli A, *et al*. *CFTR* and *FOXO1* gene expression are reduced and high mobility group box 1 (HMGB1) is increased in the ovaries and serum of women with polycystic ovarian syndrome. Gynecological Endocrinology: the Official Journal of the International Society of Gynecological Endocrinology. 2019; 35: 842–846. https://doi.org/10.1080/09513590.2019.1599349.

[10] Ni XR, Sun ZJ, Hu GH, Wang RH. High concentration of insulin promotes apoptosis of primary cultured rat ovarian granulosa cells via its increase in extracellular HMGB1. Reproductive Sciences (Thousand Oaks, Calif.). 2015; 22: 271–277. https://doi.org/10.1177/1933719114549852.

[11] Yang Y, Yang L, Qi C, Hu G, Wang L, Sun Z, *et al*. Cryptotanshinone alleviates polycystic ovary syndrome in rats by regulating the HMGB1/TLR4/NF-κB signaling pathway. Molecular Medicine Reports. 2020; 22: 3851–3861. https://doi.org/10.3892/mmr.2020.11469.

[12] Zhu HL, Chen YQ, Zhang ZF. Downregulation of lncRNA ZFAS1 and upregulation of microRNA-129 repress endocrine disturbance, increase proliferation and inhibit apoptosis of ovarian granulosa cells in polycystic ovarian syndrome by downregulating HMGB1. Genomics. 2020; 112: 3597–3608. https://doi.org/10.1016/j.ygeno.2020.04.011.

[13] Otoo A, Czika A, Lamptey J, Yang JP, Feng Q, Wang MJ, *et al*. Emodin improves glucose metabolism and ovarian function in PCOS mice via the HMGB1/TLR4/NF-κB molecular pathway. Reproduction (Cambridge, England). 2023; 166: 323–336. https://doi.org/10.1530/REP-22-0449.

[14] Motohashi H, Yamamoto M. Nrf2-Keap1 defines a physiologically important stress response mechanism. Trends in Molecular Medicine. 2004; 10: 549–557. https://doi.org/10.1016/j.molmed.2004.09.003.

[15] Ji R, Jia F, Chen X, Gao Y, Yang J. Carnosol inhibits KGN cells oxidative stress and apoptosis and attenuates polycystic ovary syndrome phenotypes in mice through Keap1-mediated Nrf2/HO-1 activation. Phytotherapy Research: PTR. 2023; 37: 1405–1421. https://doi.org/10.1002/ptr.7749.

[16] Li Y, Xu J, Li L, Bai L, Wang Y, Zhang J, *et al*. Inhibition of Nicotinamide adenine dinucleotide phosphate oxidase 4 attenuates cell apoptosis and oxidative stress in a rat model of polycystic ovary syndrome through the activation of Nrf-2/HO-1 signaling pathway. Molecular and Cellular Endocrinology. 2022; 550: 111645. https://doi.org/10.1016/j.mce.2022.111645.

[17] Ji R, Jia FY, Chen X, Wang ZH, Jin WY, Yang J. Salidroside alleviates oxidative stress and apoptosis via AMPK/Nrf2 pathway in DHT-induced human granulosa cell line KGN. Archives of Biochemistry and Biophysics. 2022; 715: 109094. https://doi.org/10.1016/j.abb.2021.109094.

[18] Taheri M, Hayati Roudbari N, Amidi F, Parivar K. The protective effect of sulforaphane against oxidative stress in granulosa cells of patients with polycystic ovary syndrome (PCOS) through activation of AMPK/AKT/NRF2 signaling pathway. Reproductive Biology. 2021; 21: 100563. https://doi.org/10.1016/j.repbio.2021.100563.

[19] Han WM, Hong YX, Xiao GS, Wang RY, Li G. NMDARs activation regulates endothelial ferroptosis via the PP2A-AMPK-HMGB1 axis. Cell Death Discovery. 2024; 10: 34. https://doi.org/10.1038/s41420-023-01794-3.

[20] Wang F, Qi Y, Gao Y, Wang Z, Shen X, Wu H. Syringic acid suppresses ferroptosis of skeletal muscle cells to alleviate lower limb ischemia/reperfusion injury in mice via the HMGB1 pathway. Chemical Biology & Drug Design. 2023; 102: 1387–1398. https://doi.org/10.1111/cbdd.14326.

[21] Davaanyam D, Lee H, Seol SI, Oh SA, Kim SW, Lee JK. HMGB1 induces hepcidin upregulation in astrocytes and causes an acute iron surge and subsequent ferroptosis in the postischemic brain. Experimental & Molecular Medicine. 2023; 55: 2402–2416. https://doi.org/10.1038/s12276-023-01111-z.

[22] Zhang H, Wang Z, Liu Z, Du K, Lu X. Protective Effects of Dexazoxane on Rat Ferroptosis in Doxorubicin-Induced Cardiomyopathy Through Regulating HMGB1. Frontiers in Cardiovascular Medicine. 2021; 8: 685434. https://doi.org/10.3389/fcvm.2021.685434.

[23] Gao Z, Hu Y, Fu H, Jiang F, Yan H, Yang X, *et al*. Dasatinib causes keratinocyte apoptosis via inhibiting high mobility group Box 1-mediated mitophagy. Toxicology Letters. 2023; 373: 22–32. https://doi.org/10.1016/j.toxlet.2022.11.004.

[24] Bhat SM, Massey N, Shrestha D, Karriker LA, Jelesijević T, Wang C, *et al*. Transcriptomic and ultrastructural evidence indicate that anti-HMGB1 antibodies rescue organic dust-induced mitochondrial dysfunction. Cell and Tissue Research. 2022; 388: 373–398. https://doi.org/10.1007/s00441-022-03602-3.

[25] Yang L, Ye F, Zeng L, Li Y, Chai W. Knockdown of HMGB1 Suppresses Hypoxia-Induced Mitochondrial Biogenesis in Pancreatic Cancer Cells. OncoTargets and Therapy. 2020; 13: 1187–1198. https://doi.org/10.2147/OTT.S234530.

[26] Taylor OJ, Thatcher MO, Carr ST, Gibbs JL, Trumbull AM, Harrison ME, *et al*. High-Mobility Group Box 1 Disrupts Metabolic Function with Cigarette Smoke Exposure in a Ceramide-Dependent Manner. International Journal of Molecular Sciences. 2017; 18: 1099. https://doi.org/10.3390/ijms18051099.

[27] Feng Z, Wang JW, Wang Y, Dong WW, Xu ZF. Propofol Protects Lung Endothelial Barrier Function by Suppression of High-Mobility Group Box 1 (HMGB1) Release and Mitochondrial Oxidative Damage Catalyzed by HMGB1. Medical Science Monitor: International Medical Journal of Experimental and Clinical Research. 2019; 25: 3199–3211. https://doi.org/10.12659/MSM.915417.

[28] Niu C, Jiang D, Guo Y, Wang Z, Sun Q, Wang X, *et al*. Spermidine suppresses oxidative stress and ferroptosis by Nrf2/HO-1/GPX4 and Akt/FHC/ACSL4 pathway to alleviate ovarian damage. Life Sciences. 2023; 332: 122109. https://doi.org/10.1016/j.lfs.2023.122109.

[29] Chen X, Song QL, Li ZH, Ji R, Wang JY, Cao ML, *et al*. Pterostilbene ameliorates oxidative damage and ferroptosis in human ovarian granulosa cells by regulating the Nrf2/HO-1 pathway. Archives of Biochemistry and Biophysics. 2023; 738: 109561. https://doi.org/10.1016/j.abb.2023.109561.

[30] Wang C, Chen S, Guo H, Jiang H, Liu H, Fu H, *et al*. Forsythoside A Mitigates Alzheimer's-like Pathology by Inhibiting Ferroptosis-mediated Neuroinflammation via Nrf2/GPX4 Axis Activation. International Journal of Biological Sciences. 2022; 18: 2075–2090. https://doi.org/10.7150/ijbs.69714.

[31] Cai X, Hua S, Deng J, Du Z, Zhang D, Liu Z, *et al*. Astaxanthin Activated the Nrf2/HO-1 Pathway to Enhance Autophagy and Inhibit Ferroptosis, Ameliorating Acetaminophen-Induced Liver Injury. ACS Applied Materials & Interfaces. 2022; 14: 42887–42903. https://doi.org/10.1021/acsami.2c10506.

[32] Holmström KM, Kostov RV, Dinkova-Kostova AT. The multifaceted role of Nrf2 in mitochondrial function. Current Opinion in Toxicology. 2016; 1: 80–91. https://doi.org/10.1016/j.cotox.2016.10.002.

[33] Li Y, Feng YF, Liu XT, Li YC, Zhu HM, Sun MR, *et al*. Songorine promotes cardiac mitochondrial biogenesis via Nrf2 induction during sepsis. Redox Biology. 2021; 38: 101771. https://doi.org/10.1016/j.redox.2020.101771.

[34] Liu Z, Wang J, Jin X, Gao P, Zhao Y, Yin M, *et al*. 1,8-Cineole Alleviates OGD/R-Induced Oxidative Damage and Restores Mitochondrial Function by Promoting the Nrf2 Pathway. Biological & Pharmaceutical Bulletin. 2023; 46: 1371–1384. https://doi.org/10.1248/bpb.b23-00154.

[35] Jin SH, Sun JJ, Liu G, Shen LJ, Weng Y, Li JY, *et al*. Nrf2/PHB2 alleviates mitochondrial damage and protects against *Staphylococcus aureus*-induced acute lung injury. MedComm. 2023; 4: e448. https://doi.org/10.1002/mco2.448.

[36] Zhu H, Dai Z, Liu X, Zhou H, Wang Y. Serine/threonine kinase 3 promotes oxidative stress and mitochondrial damage in septic cardiomyopathy through inducing Kelch-like ECH-associated protein 1 phosphorylation and nuclear factor erythroid 2-related factor 2 degradation. International Journal of Biological Sciences. 2023; 19: 1369–1381. https://doi.org/10.7150/ijbs.80800.